

**Sulfate formation via aerosol phase SO₂ oxidation by model biomass
burning photosensitizers: 3,4-dimethoxybenzaldehyde, vanillin and
syringaldehyde using single particle mixing state analysis**

Liyuan Zhou^{1,2}, Zhancong Liang^{1,2}, Beatrix Rosette Go Mabato^{1,2}, Rosemarie Ann Infante Cuevas^{1,2},
Rongzhi Tang^{1,2}, Mei Li^{3,4}, Chunlei Cheng^{3,4} and Chak K. Chan^{1,2,5*}

¹School of Energy and Environment, City University of Hong Kong, Hong Kong, China

²City University of Hong Kong Shenzhen Research Institute, Shenzhen, China

³Institute of Mass Spectrometry and Atmospheric Environment, Guangdong Provincial Engineering Research Center for On-line Source Apportionment System of Air Pollution, Jinan University, Guangzhou 510632, China

⁴Guangdong-Hongkong-Macau Joint Laboratory of Collaborative Innovation for Environmental Quality, Guangzhou 510632, China

⁵Low-Carbon and Climate Impact Research Centre of School of Energy and Environment, City University of Hong Kong, Hong Kong, China

Correspondence to: Chak K. Chan (Chak.K.Chan@cityu.edu.hk)

Abstract. Atmospheric oxidation of sulfur dioxide (SO₂) to sulfate has been widely investigated by means of gas phase and in-cloud chemistry studies. Recent field measurements have shown significant sulfate formation in cloud-free environments with high aerosol loadings. As an important fraction of biomass burning aerosol components, particulate phenolic and non-phenolic aromatic carbonyls may initiate photosensitized aerosol multiphase oxidation of SO₂, of which our knowledge however is still in its nascent stage. In this study, on the basis of single-particle aerosol mass spectrometry (SPAMS) measurements, we find evident sulfate formation in the biomass burning-derived photosensitizer particles under UV and SO₂ exposure, attributable to photosensitized oxidation of S(IV), while almost no sulfate was observed under dark and existence of SO₂. The efficiency of sulfate production under UV irradiation, represented by the number percentage of sulfate-containing particles (99-43%) and sulfate relative peak area (RPA) (0.67-0.12) in single particle spectra, in descending order, were 3,4-dimethoxybenzaldehyde (DMB), vanillin (VL) and syringaldehyde (SyrAld). Internal mixtures of VL and potassium nitrate gave a slightly lower number percentage and RPA of sulfate than VL particles alone. In externally mixed VL and potassium nitrate particles, sulfate was predominantly formed on the former, confirming that sulfate formation via photosensitization prevails over that via nitrate photolysis. Our results suggest that photosensitized oxidation of S(IV) could make an important contribution to aerosol sulfate formation, especially in areas influenced by biomass burning.

1. Introduction

Sulfate is a key component of fine particulate matter in the atmosphere, which impacts air quality, climate, and human and ecosystem health (Nel, 2005; Fuzzi et al., 2015; Grantz et al., 2003). Traditional atmospheric models, including the gas-phase oxidation of sulfur dioxide (SO₂) by hydroxyl radical (OH) (Calvert et al., 1978) and stabilized Criegee intermediates (Cheng et al., 2016) and a series of aqueous, in-cloud oxidation of SO₂, underpredict the sulfate production during heavy pollution episodes in China (Zheng et al., 2015; Zhang et al., 2015; Wang et al., 2014; Liu and Abbatt, 2021). Although the liquid water content (LWC) is generally much lower in aerosol particles than in fog and cloud droplets, it was reported that aerosol multiphase oxidation processes are important, especially in polluted and high relative humidity (RH) conditions (Liu et al., 2021; Liu et al., 2020). The typical oxidants involved in multiphase oxidation of S(IV) in aerosol particles include dissolved ozone (O₃) (Hoffmann and Calvert, 1985), hydrogen peroxide (H₂O₂) (Hoffmann and Calvert, 1985), transition metal ions

44 (TMIs, i.e., Fe (III) and Mn(II)) (Ibusuki and Takeuchi, 1987; Harris et al., 2013; Alexander et al., 2009; Martin and Good,
45 1991), methyl hydrogen peroxide (Walcek and Taylor, 1986) and peroxyacetic acid (Walcek and Taylor, 1986). To narrow the
46 gap between the measured and modeled sulfate production, new chemical pathways have been suggested involving nitrogen
47 dioxide (NO₂) (Wang et al., 2016; Cheng et al., 2016), organic peroxides (Yao et al., 2019; Ye et al., 2018), oxidants from
48 particulate nitrate photolysis (Gen et al., 2019a, b; Zhang et al., 2020), and hypohalous acid (HOX, e.g., HOCl and HOBr) (Liu
49 and Abbatt, 2020). However, the missing sulfate source has still remained unclear and controversial.

50 Photosensitization in atmospheric aerosols has been recently proposed to initiate novel chemistry in the formation of
51 secondary pollutants (George et al., 2015). Upon irradiation, atmospheric photosensitizers such as aromatic carbonyls can
52 generate triplet excited states (³C*) (Canonica et al., 1995; Anastasio et al., 1996; Smith et al., 2014; Kaur and Anastasio,
53 2018; Kaur et al., 2019; Smith et al., 2016), which can oxidize phenols at higher rates compared to OH, particularly under
54 acidic conditions (Smith et al., 2014). In addition to being an oxidant, ³C* can also react with O₂ to generate secondary
55 oxidants, such as singlet oxygen (¹O₂), superoxide (O₂^{•-}), hydroperoxyl radical ([•]HO₂), and hydroxyl radicals ([•]OH) (Corral
56 Arroyo et al., 2018; Dalrymple et al., 2010; George et al., 2018). Biomass burning is an important source of aromatic
57 carbonyls (Rogge et al., 1998; Nolte et al., 2001; Schauer et al., 2001), and the concentrations of phenolic and non-phenolic
58 carbonyls are comparable in biomass burning smoke (Simoneit et al., 1993; Anastasio et al., 1996). Direct photosensitized
59 oxidation of vanillin (a typical aromatic carbonyl photosensitizer) has been reported as an important pathway to form aqueous
60 secondary organic aerosol in areas influenced by biomass burning, with reaction products dominated by brown carbon
61 chromophores (Mabato et al., 2022; Mabato et al., 2023). However, only limited studies focused on the role of biomass
62 burning-derived photosensitizers in S(IV) oxidation. Wang et al. (2020) reported that photosensitized chemistry involving the
63 humic fraction of aerosols during Chinese haze events could explain a significant fraction of the observed sulfate formation,
64 which highlighted the potential photosensitizing properties played by biomass burning particles. Naphthalene, emitted
65 primarily from fossil fuel combustion and biomass burning, can be oxidized by hydroxyl radicals to form secondary organic
66 aerosol (SOA), which was observed to possess interfacial photosensitizing properties (Wang et al., 2021). These recent studies
67 have advanced our understanding of the photosensitized processes, but the types of photosensitizers from biomass burning are
68 diverse and their properties are complex, limiting us from further assessing the importance of photosensitized sulfate formation

in the dynamic ambient atmosphere. In this study, we investigate sulfate formation via aerosol phase SO₂ oxidation by biomass burning-derived aromatic carbonyl photosensitizers, including both non-phenolic (3,4-dimethoxybenzaldehyde, DMB) and phenolic photosensitizers (vanillin, VL and syringaldehyde, SyrAld) with similar molar absorptivity at atmospheric relevant wavelengths (Figure S1, Supporting information), in an oxidation flow reactor (OFR) utilizing a single particle aerosol mass spectrometer (SPAMS). Nitrate photolysis has been reported as a typical sulfate formation pathway initiated by particulate photoactive compounds, similar to photosensitization (Gen et al., 2022). The objectives of this study are to semi-quantitatively evaluate the extent of sulfate formation in photosensitizer particles and qualitatively compare the relative atmospheric importance of particulate photosensitization and nitrate photolysis in sulfate formation.

2. Methods

2.1 Materials and experimental setup

A vaporization - condensation method was used to coat photosensitizing or non-photosensitizing species on 0.3 μm polystyrene latex sphere (PSL) particles (Thermo Fisher Scientific Inc., MA) (Qi et al., 2019). A detailed experimental setup is shown in Figure S2a and the initial experimental conditions are summarized in Table S1. All chemicals, including DMB (Acros Organics, 99+%), VL (Acros Organics, 99%), SyrAld (Sigma Aldrich, 98%), benzoic acid (BA, Acros Organics, 99.6%), potassium nitrate (KNO₃, Sigma Aldrich, 99+%) and oxalic acid (Sigma Aldrich, 99.9+%) were used as purchased. The structures of the chemicals used are provided in Table S2. PSL particles were selected as condensation nuclei due to their chemically and thermally inert nature. Their size did not change upon passing through the dryer or glass bottle at 120°C oil bath or exposure to SO₂ or UV irradiation (Figure S3). In addition, PSL particles are difficult to be ionized and do not complicate the interpretation of mass spectra. PSL condensation nuclei were generated by using a constant output atomizer (TSI 3076) with pure N₂ gas (>99.995 %), and a portion of the particles passed through a diffusion dryer at a flow rate of 300 mL min⁻¹ to achieve RH <10%. The dried particles subsequently passed through a heated glass bottle (inlet about 2 inches above the bottom) containing ~0.5g of either DMB, VL, SyrAld or BA at the bottom. The heating temperatures of the glass bottle were regulated using an oil bath near the melting points of the chemicals. The generated organic vapor condensed to form coatings onto the PSL particles. The coating thickness was estimated by the measured particle size increase by the

94 SPAMS. For control experiments with PSL-only particles, the particles passed through the same glass bottle containing no
95 chemicals. Photosensitizing (DMB, VL, SyrAld) (Smith et al., 2015, 2016; Smith et al., 2014) and non-photosensitizing
96 (BA) (Smith et al., 2015) species coated particles or uncoated PSL-only particles were then introduced into an OFR (volume
97 of approximately 7.2 L) and mixed with SO₂ gas. SO₂ was delivered by a flow of around 11 mL min⁻¹ (203 ppm, mixing with
98 pure N₂, Scientific Gas Engineering Co., Ltd.) to achieve the SO₂ concentration of around 750 ppb in the OFR. Depending on
99 the experiment, the RH in the OFR was regulated at ~80% or 20% to achieve different content of aerosol water by passing
100 HEPA-filtered and activated-carbon-denuded compressed air or pure N₂ through water bubblers. Note that the photosensitizers
101 may be (polymorphic) solid or semi-solid due to their low solubility and hygroscopicity, even at 80% RH (Kavuru et al., 2016;
102 Hussain et al., 2001). For example, Mochida and Kawamura (2004) reported that pyrolysis products of lignin with -COOH,
103 including vanillic acid and syringic acid, showed no hygroscopic growth even at RH of more than 90%. They also proposed
104 that other pyrolysis products with chemical structures such as -CHO may have even lower hygroscopicity than -COOH and
105 would not show measurable particle growth. Though we could not observe the phase states of the particles, both aerosol liquid
106 water in (partially) deliquescent particles and surface adsorbed water content on solid particles at 80% RH were expected to
107 be higher than at 20% RH (Rubasinghege and Grassian, 2013). Experiments under air enable the generation of secondary
108 oxidants. Conversely, the N₂ experiments would inhibit the formation of secondary oxidants, which can lead to triplets-driven
109 reactions (Chen et al., 2020). The total flow in the OFR was around 3 L min⁻¹, resulting in a residence time of ~ 2.5 min. There
110 are four UVA lamps (Shenzhen Guanhongrui Technology Co., Ltd.) with a continuous emission spectrum over 310-420 nm
111 surrounding the OFR. We conducted experiments with one and four lamps to provide a total irradiance of about 1.1×10¹⁵ (I₁)
112 and 3.8×10¹⁵ (I₄) photon cm⁻² s⁻¹, respectively (see details in Supporting information, Text S1); and dark control experiments
113 were performed with UV lamps off. Each experiment lasted around 20 minutes. In the absence of light and SO₂, there was no
114 change in the mass spectra of coated particles (Figure S4). At the outlet of the OFR, SO₂ concentration was monitored by a
115 SO₂ analyzer (Teledyne, T100, USA), and the size and chemical composition of individual aerosol particles were analyzed by
116 a single particle aerosol mass spectrometry (SPAMS, Hexin Analytical Instrument Co., Ltd, China). This single particle
117 technique allows us to study the mixing state of the particles. KNO₃ was widely observed in biomass burning plumes (Zauscher
118 et al., 2013). Internally mixed particles of photosensitizing species and KNO₃ were generated by atomizing aqueous solutions

of KNO_3 with several drops of PSL suspension, followed by passing through a dryer and then the heated glass bottle containing photosensitizing species as described above (Figure S2a). Externally mixed particles were generated with a second atomizer (TSI 9032), and the generated KNO_3 or KNO_3 -oxalic acid mixed particles were mixed with photosensitizing species coated particles in a stainless-steel chamber ($\phi 3 \times 8''$) before introduction to the OFR (Figure S2b).

2.2 SPAMS and data analysis

A detailed description of the operational principle of SPAMS has been provided elsewhere (Li et al., 2011). Briefly, aerosol particles were introduced into the SPAMS through an orifice and aerodynamic lens and consecutively irradiated by two laser beams, where their aerodynamic diameter were determined through the velocity and flight time. The sized particles were then desorbed and ionized by a pulsed 266 nm laser (0.5 mJ), which was triggered at the precise time on the basis of the particle velocities. The produced positive and negative molecular fragments were analyzed by a Z-shaped bipolar time-of-flight mass spectrometer (Pratt et al., 2009; Li et al., 2011). The ionization efficiency of SPAMS to detect 250-2000 nm atmospheric aerosol particles was above 30% on average (Li et al., 2011). The number of ionized particles for each experiment condition was around 1000-3000, sufficient for systematically identifying the heterogeneous reaction products (Liang et al., 2022; Qi et al., 2019). Furthermore, each experiment was repeated, as reflected in Figure S6. Single particle size and mass spectral analysis were performed using the Computational Continuation Core (COCO) toolkit based on MATLAB software. The number percentage and relative peak area (RPA, defined as the fractional contribution of the targeted ion peak area to the sum of all ion peak areas) were applied to indicate the variations of the amount of different species (e.g., sulfate) in individual particles (Hu et al., 2022). Sulfate-containing particles were distinguished by m/z -97 [HSO_4^-] or m/z -96 [SO_4^-] (Guazzotti et al., 2001; Liang et al., 2022). In addition, an adaptive resonance theory based neural network algorithm (ART-2a) (Li et al., 2011) was used to separate and cluster particles in external and internal mixtures according to the similarities in individual mass spectra of single particles. Before entering the SPAMS, the particles passed through a diffusion dryer to reduce the matrix effects from water (Neubauer et al., 1998).

144 3. Results and discussion

145 Photosensitized SO₂ uptake and sulfate formation

146 Figure 1a shows the changes in SO₂ concentration ([SO₂]) in the presence of PSL particles coated with various types of
147 photosensitizing (DMB, VL and SyrAld) and non-photosensitizing (BA) species under dark and UV irradiation conditions. In
148 Figure 1a, for UV condition, only time traces of SO₂ under I₄ UV irradiance were shown for clarity, and I₁ UV irradiance cases
149 can be found in Figure S5. Except stated otherwise, results shown in the following discussions were obtained at 80% RH. The
150 steady concentration of SO₂ in the OFR was at around 750 ppb under dark conditions. Upon exposure to UV light, a rapid drop
151 in the SO₂ concentration was observed in the presence of DMB- and VL-coated particles, indicating photoinduced uptake of
152 SO₂ on these particles. Wang et al. (2021) suggested that the photosensitized chemical reactions between naphthalene-derived
153 SOA and SO₂ likely occur at/near the particle surface. In this study, the SO₂ consumption under UV irradiation for DMB and
154 VL coated particles increased with the surface area of SPAMS detected particles in the OFR (Figure 1a and S6) ($R^2=0.84$ -
155 0.99). Total surface area concentrations in the range of 7×10^4 - 2×10^5 $\mu\text{m}^2\text{ m}^{-3}$ are denoted by “small”, in 2×10^5 - 6×10^5 μm^2
156 m^{-3} as “medium”, and larger than 6×10^5 $\mu\text{m}^2\text{ m}^{-3}$ as “large”. These values fall within the urban background and indoor air
157 ranges but are slightly lower than urban pollution ranges (Willeke and Whitby, 1975; Hudda and Fruin, 2016; Qi et al., 2008).
158 SO₂ consumption per unit surface area concentration also increased with higher UV irradiance (Figure S6). Only slight SO₂
159 consumption under UV irradiation was observed in the presence of SyrAld-coated particles and no observable decrease in SO₂
160 concentrations in the absence of photosensitizing species, i.e., BA-coated particles and PSL-only particles, was found. The
161 average mass spectra of DMB-, VL-, SyrAld- and BA-coated single particles under dark and UV irradiation in the presence of
162 SO₂ are shown in Figure 1b, characterized by their respective parent ions (in either neutral, protonated or deprotonated form)
163 and expected smaller organic fragment ions. PSL-only particles do not ionize and no mass spectra were observed (Qi et al.,
164 2019). No sulfate was formed under dark condition, consistent with the stable SO₂ concentrations observed. However, upon
165 exposure to UV irradiation, the RPA of sulfate ($^{97}\text{HSO}_4^-$ and $^{96}\text{SO}_4^-$) increased significantly, accompanied by the slight decrease
166 of RPA of the parent ions of $^{165}\text{C}_9\text{H}_9\text{O}_3^{+/-}$, $^{153}\text{C}_8\text{H}_9\text{O}_3^{+/-}$, $^{181}\text{C}_9\text{H}_9\text{O}_4^{+/-}$ for DMB-, VL- and SyrAld-coated particles respectively.
167 Mabato et al. (2022) reported direct photosensitized oxidation of photosensitizers, which can generate oxygenated products

168 such as functionalized monomers and oxygenated ring-opening products. In this study, we observed the peak of $^{181}\text{C}_9\text{H}_9\text{O}_4^+$
169 (DMB+O) upon UV irradiation, but the identification of organic products was generally limited by laser-induced fragmentation
170 in the SPAMS. Although the coating thickness estimated by particle size increase spanned a wide range from 100 nm to 2.2
171 μm , the number percentage and RPA of sulfate generally exhibited the same trend for the studied photosensitizers in each size
172 bin (Figures S7). Figure 2 shows the average RPA of sulfate (circles) and the number percentage of sulfate-containing particles
173 (diamonds) in DMB-, VL-, SyrAld- and BA-coated particles at dark and different UV intensities in the presence of SO_2 , and
174 the corresponding SO_2 consumption normalized by the average total particle surface area concentration before and after UV
175 irradiation in the OFR detected by SPAMS (crosses). The RPA and number percentage of sulfate for each experimental
176 condition were calculated by taking the average of those values in different size bins in Figure S7. Hence the potential uneven
177 coating thickness has been incorporated in the averages, which show consistent trends in Figure 2. The average number
178 percentages of sulfate-containing particles in DMB- and VL- coated particles are considerably higher ($> 84\%$) under both I_1
179 and I_4 UV irradiances than under dark ($< 2\%$). SyrAld-coated particles gave a slightly lower percentage of sulfate-containing
180 particles of 43% and 83% at I_1 and I_4 UV irradiances. Upon increase of photon flux densities (I_1 to I_4), the RPA of sulfate
181 increases for DMB-, VL- and SyrAld-coated particles, which is in line with the enhanced normalized SO_2 consumptions. The
182 number percentage and RPA of sulfate exhibited a similar descending order of $\text{DMB} > \text{VL} > \text{SyrAld} > \text{BA}$ in each size bin (Figure
183 S7). The pHs of the DMB (6.01 ± 0.06), VL (6.15 ± 0.12) and SyrAld (5.97 ± 0.10) particles were similar. Our observed trend of
184 sulfate formation potential is in line with the secondary organic aerosol mass yield for syringol oxidation by $^3\text{C}^*$ of DMB
185 (114%), VL (111%) and SyrAld (78%) in the literature (Smith et al., 2016; Smith et al., 2014). Specifically, DMB has a higher
186 quantum yield and longer lifetime of $^3\text{C}^*$ compared to VL (Felber et al., 2021), which can result in a higher sulfate formation
187 efficiency. On the other hand, the direct photodegradation rate constant was higher for SyrAld than VL, likely suppressing the
188 concentration of SyrAld in droplets/ particles and the photosensitized oxidation (Smith et al., 2016). However,
189 photosensitization is still a research field for atmospheric chemistry with broad uncertainties (Felber et al., 2021). Further
190 quantitative work on the quantum yield, lifetime, and the decay and quenching rate constants of the $^3\text{C}^*$ is needed.

191 The loss of SO_2 associated with the synchronous sulfate production in single DMB-, VL- and to a lesser extent,
192 SyrAld-coated particles was likely attributed to the photosensitization-induced oxidation of S(IV) (i.e., SO_2 , HSO_3^- , and SO_3^{2-}).

Specifically, UV irradiation could excite photosensitizers from their ground state to singlet excited state, then rapidly relax to a triplet state via intersystem crossing (George et al., 2015; Gomez Alvarez et al., 2012). S(IV) could be oxidized to sulfate directly by $^3\text{C}^*$, or by the secondary oxidants (e.g., $^1\text{O}_2$, $\text{O}_2^{\bullet-}/\text{HO}_2$ and $\cdot\text{OH}$) produced from the excited molecules and O_2/water . Wang et al. (2020) observed sulfate production from direct reactions between triplets of 4-(benzoyl) benzoic acid, humic acid and their salts, and hydrated S(IV).

In our previous study, we have reported the enhanced SO_2 oxidation and sulfate formation in incense and mosquito coil burning particles (Liang et al., 2022), as surrogates of biomass burning organic aerosol, BBOA (Li et al., 2012; Zhang et al., 2014), under light, when compared with dark conditions. The number percentage of sulfate-containing particles increased from around 50% under dark to around 90% after UV irradiation (Figure 2). Incense burning particles contain a variety of photosensitizers, e.g., DMB, VL and SyrAld (Peng et al., 2020; Liu and Sun, 1988; Liang et al., 2022), which could oxidize SO_2 via photosensitization. In contrast to Liang et al. (2022), we did not observe sulfate formation under dark in the current study. Their much higher percentage of sulfate-containing particles under dark was likely due to the gaseous oxidants in incense-burning plumes in their experiments. Furthermore, as mentioned earlier, in the control experiment using BA-coated particles as seeds in the presence of SO_2 , neither the RPA of sulfate nor the number percentage of sulfate-containing particles changed upon irradiation. This indicates that the direct photoexcitation of SO_2 in the presence of water leading to the formation of OH and subsequently sulfate plays a negligible role (Kroll et al., 2018; Martins-Costa et al., 2018; Wang et al., 2021).

The potential role of secondary oxidants

The triplet excited state ($^3\text{C}^*$) of aromatic carbonyls can react with O_2 in air-saturated conditions via either energy transfer to form $^1\text{O}_2$ or electron transfer to form $\text{O}_2^{\bullet-}$, which can further react with H^+ ion to produce H_2O_2 and $\cdot\text{OH}$ (Dalrymple et al., 2010). Therefore, the absence of O_2 in N_2 saturated experiments would inhibit the formation of secondary oxidants. Figure 3 shows that replacing air by pure N_2 substantially shifted the distribution of RPA for DMB- and VL-coated particles toward the lower end, while SyrAld-coated particles exhibited slight changes. For example, DMB-coated particles with sulfate RPA larger than 0.6 were dominant and comprised more than 52% of total particles in air, but sulfate RPA of 0-0.2 accounts for more than 73% of the total particles in N_2 under both UV irradiances. This suggests the involvement of O_2 and the

potentially important role of secondary oxidants in sulfate formation. Upon the increase of UV intensity (from I_1 to I_4), the number fraction of particles with sulfate RPA larger than 0.2 only slightly increased in N_2 -saturated conditions, and particles with RPA of 0-0.2 dominated the population, indicating the lower ability of direct $^3C^*$ oxidation of SO_2 to produce large sulfate RPA. The relative importance of the direct $^3C^*$ and secondary oxidants in sulfate production varies among the different compounds, as reflected by the distribution of sulfate RPA in Figure 3. For example, secondary oxidants could be more important in the DMB system than the SyrAld system. In contrast, Wang et al. (2020) reported that switching from air to N_2 resulted in similar S(IV) oxidation rates, indicating that the direct reaction of SO_2 with $^3C^*$ was more significant than that with the secondary oxidants for 4-(benzoyl)benzoic acid. This discrepancy is possibly due to the different reactivities of $^3C^*$ from different photosensitizing chemicals towards SO_2 (Wang et al., 2020). In air, DMB-coated particles exhibited the strongest SO_2 oxidation potential with 88% of the total particles having sulfate RPA larger than 0.2 (I_1), followed by VL- (41%) and SyrAld- (15%) coated particles. Upon exposure to simulated sunlight, SyrAld and VL have been shown to undergo apparent direct photodegradation, but DMB exhibits smaller or almost no loss in illuminated solution mixed with non-carbonyl phenols or benzene-diols (Smith et al., 2016, 2015; Smith et al., 2014; Mabato et al., 2023; Mabato et al., 2022). This is generally consistent with the decrease of RPA of parent ions in this study (Figure S8). The rapid direct photodegradation of phenolic carbonyls (VL and SyrAld) can reduce their concentrations in the particles and limits the formation of sulfate.

Relative importance of particulate photosensitization and nitrate photolysis in sulfate formation

Nitrate is a ubiquitous constituent of atmospheric aerosol particles (Chan and Yao, 2008). Multiphase photochemical oxidation of SO_2 by the photolysis of particulate nitrate could make an important contribution to aerosol sulfate formation (Gen et al., 2019b, a). To qualitatively compare the relative atmospheric importance of photosensitization and nitrate photolysis in sulfate formation, external mixtures of VL-coated particles and KNO_3 particles were exposed to SO_2 and UV irradiation at 80% RH. VL was used for comparison owing to its moderate sulfate formation potential among the three photosensitizers tested. Potassium was the dominant cation in biomass burning plumes (Jahn et al., 2021; Freney et al., 2009; Zhang et al., 2022), and therefore KNO_3 was selected as the model nitrate salt. RPA of sulfate for VL-coated particles and KNO_3 particles at different sizes in the external mixture were compared in Figure 4a. VL-coated particles exhibited an average sulfate RPA of 0.26, with

an overall inverse relationship with particle size, while the sulfate absolute peak areas (APA) are moderately higher for large particles. The APA is proportional to the absolute number of ions detected and a larger sulfate APA may indicate a larger amount of sulfate formed. However, APA is more sensitive to the variability in ion intensities associated with particle-laser interactions than RPA (Gross et al., 2000; Hatch et al., 2014; Zhou et al., 2022). The variation in RPA was smaller than that in the APA, even though some studies found that the RPA values may also be affected by the inherent variability of particle compositions due to matrix effects within particles (Reinard and Johnston, 2008; Zhou et al., 2016). The reactive uptake comprises the diffusion of SO₂ molecules, followed by oxidation of SO₂ at/near the surface or in the bulk of the particles. The decreased sulfate RPA with increasing particle size suggested the photosensitized sulfate formation at/near the surface of VL-coated particles, probably due to the prevalence of surface reactions or diffusional limitations of SO₂ in larger particles, especially in the poorly hygroscopic and potentially viscous VL matrix. We cannot exclude the occurrence of bulk phase reaction in the organic moiety, though it was likely less efficient than the surface reaction. In contrast, deliquescent KNO₃ particles (Figure S9) exhibited RPAs of 0, suggesting that nitrate photolysis plays a negligible role in our study, although the concentration of [NO₃⁻] in KNO₃ particles at 80% RH was estimated to be 6.3 M by AIOMFAC (<http://www.aiomfac.caltech.edu>) (Zuend et al., 2008), almost 100 times higher than the solubility of VL (~66 mM). At 80% RH, the pH of KNO₃ particles was 6.38±0.07, comparable to that of VL (pH = 6.15±0.12). Thus, pH-dependent partitioning of SO₂ is not expected to play an important role in the different sulfate formation observed for KNO₃ and VL in this study. The prevailing sulfate formation in VL particles over KNO₃ particles is likely due to the much lower integrated molar absorptivity of nitrate (~143 M⁻¹ cm⁻¹) compared to VL (2.8×10⁵ M⁻¹ cm⁻¹) over the wavelength range of 300-400 nm (Figure S1). In addition, this also excluded the possibility of sulfate formation in gas phase and small nuclei, which would be expected to have condensed/coagulated on both the photosensitizer and KNO₃ particles. When RH decreased to 20%, a significant reduction in the average RPAs from 0.26 to 0.002 was observed for VL-coated particles (Figure S10), attributable to the fewer dissolved VL for sulfate formation since VL has low solubility and hygroscopicity and the limited SO₂ dissolution (Liu et al., 2021). In addition, lower RH could result in higher particulate viscosity, which hinders molecular diffusion and reaction (Kroll et al., 2018; González Palacios et al., 2016; Corral Arroyo et al., 2018). A systematic study of the effect of RH on the particle-phase photosensitized reaction is desirable. Overall, sulfate formation was found on VL-coated particles but not on externally

mixed nitrate particles at both high and low RH in our study. Oxalic acid is one of the most abundant species of organic aerosols and is commonly found in atmospheric nitrate-containing particles (Mochizuki et al., 2017; Cheng et al., 2017; Yang et al., 2009). We have also conducted experiments with internal mixtures of KNO_3 and oxalic acid, which did not show sulfate formation as well (Figure 4b). However, internally mixed VL and KNO_3 yielded 55% sulfate-containing particles and an average sulfate RPA of 0.12. These values fall in between those of pure KNO_3 and VL-coated particles (Figure 4c). As the ion intensity ratio of nitrate to organics of the KNO_3 -VL internally mixed particles of similar size decreased, higher sulfate RPAs were found. The quantitative sulfate production rate via aerosol phase SO_2 oxidation by model photosensitizer is limited by SPAMS measurements in the current study, which focuses on single particle mixing state analysis. Further quantitative studies would be useful.

4. Environmental implications

This paper presents insights on aerosol SO_2 oxidation by biomass burning-derived photosensitizers using single particle characterization. Sulfate formation in photosensitizer coated particles, in terms of both number percentage and RPA of sulfate, was significantly higher under UV irradiation than under dark. From dark to UV irradiation, the average number percentages of sulfate-containing particles increased from less than 2% to 43-99%, and sulfate RPA increased from almost 0 to 0.12-0.67 for SyrAld, VL, and DMB-coated particles.

The speciation, concentration, and properties of photosensitizers in ambient particles are still poorly understood, limiting the parameterization of photosensitized sulfate formation. Nevertheless, we observed that sulfate formation via photosensitization is qualitatively more efficient than nitrate photolysis for wet aerosols at 80% RH. Recently, we found that incense burning particles (considered as typical BBOA surrogates) show increases of sulfate-containing particles and sulfate RPAs by ~45% and ~0.35 under UV than dark, respectively, due to photosensitization reactions of SO_2 (Liang et al., 2022). These results are within the ranges of our measurements in this paper. The SO_2 exposure of ~1800 ppb min in the OFR in this study corresponds to a 45 min and 450 min atmospheric SO_2 exposure, taking an ambient RH of 80% and SO_2 concentration

289 of 40 ppb during extreme haze events (Cheng et al., 2016) and 4 ppb in usual days (Chen et al., 2022), respectively. This
290 indicates that after exposure of tens of minutes to hours to SO₂, more than 40% of fresh BBOA particles could contain sulfate
291 via photosensitization, especially under high photon flux such as during typical clear days and haze days in Beijing, China,
292 which were around 4 and 1.4 times, respectively, of that in the OFR (I₄) (Figure S1). Our finding provides additional
293 experimental support to the potentially important contribution of photosensitized oxidation of S(IV) to aerosol sulfate
294 formation in biomass burning plumes. Future studies of the quantification and mechanism revelation of sulfate formation via
295 photosensitization are needed. In addition, we solely studied three typical biomass burning-derived photosensitizers.
296 Photosensitized sulfate formation on real BBOA particles, which is a complex matrix of organics, is to be explored further.

297

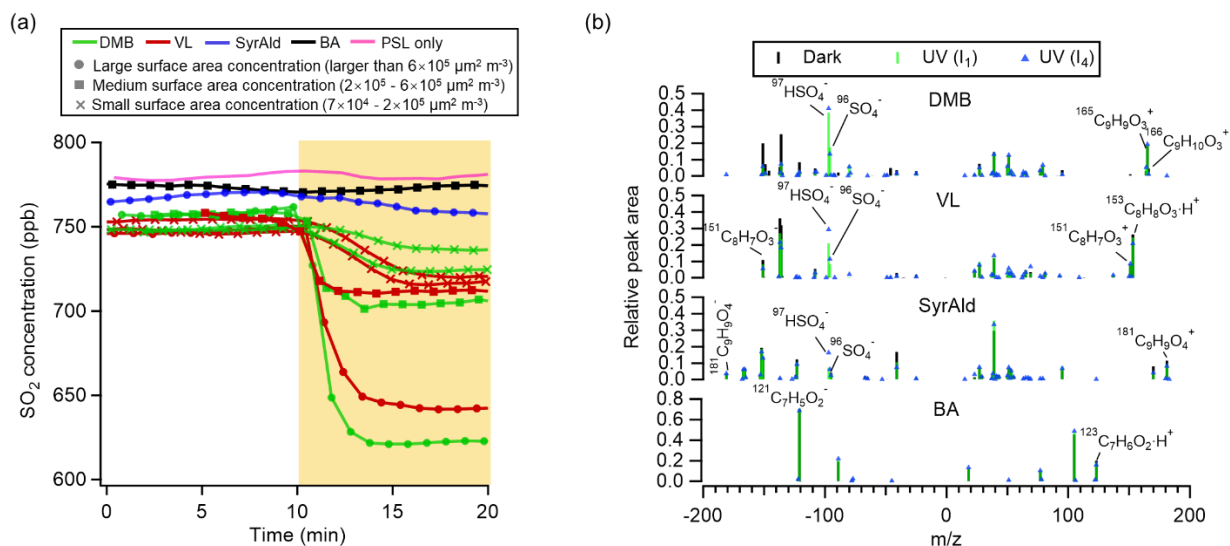


Figure 1. (a) Time traces of SO_2 in the dark (0-10 min) and under UV irradiation (I_4) (10-20 min) in the presence of DMB-, VL-, SyrAld-, or BA-coated particles and PSL-only particles. The SO_2 consumption is presented as a function of the total surface area concentration of SPAMS detected particles. Total surface area concentrations in the range of 7×10^4 - $2 \times 10^5 \mu\text{m}^2 \text{m}^{-3}$ are denoted by “small”, in 2×10^5 - $6 \times 10^5 \mu\text{m}^2 \text{m}^{-3}$ as “medium”, and larger than $6 \times 10^5 \mu\text{m}^2 \text{m}^{-3}$ as “large”. (b) Average negative and positive mass spectra for the DMB-, VL-, SyrAld- and BA-coated particles under dark and UV irradiation (I_1 and I_4) conditions. All experiments were conducted at 80% RH.

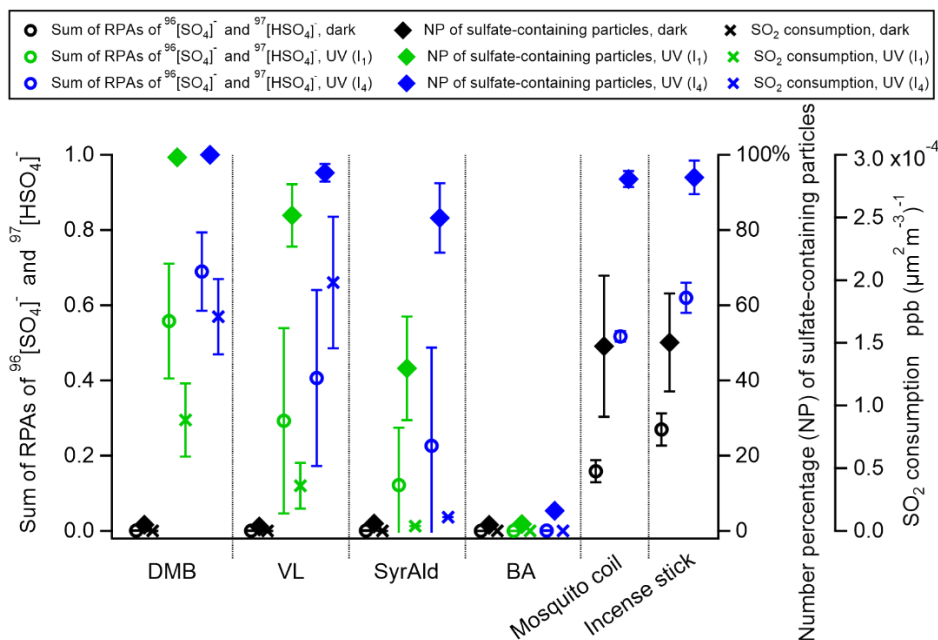


Figure 2. Average sulfate relative peak areas (RPAs), and number percentage of sulfate-containing particles for the DMB-, VL-, SyrAld- and BA-coated particles, mosquito coil burning, and incense burning particles under dark and UV irradiation conditions in the presence of SO₂. Errors are shown by 95% confidence intervals. SO₂ consumptions normalized by the average total particle surface area concentrations before and after UV irradiation in the OFR detected by SPAMS are shown. Data of incense and mosquito coil burning particles were from Liang et al. (2022). All experiments were conducted at 80% RH.

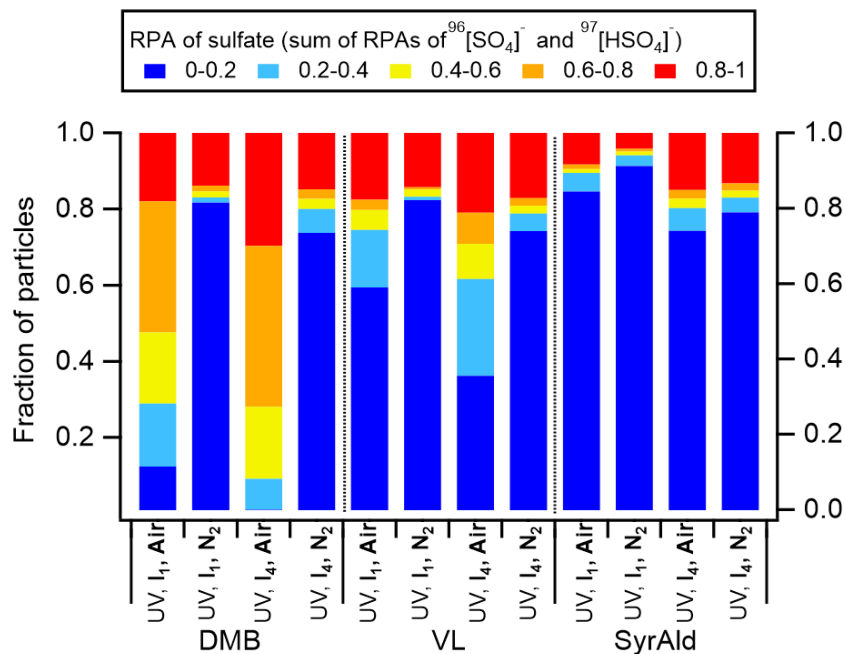


Figure 3. Distribution of sulfate RPA for DMB-, VL- and SyrAld-coated particles under air and N₂ conditions at different UV intensities in the presence of SO₂.

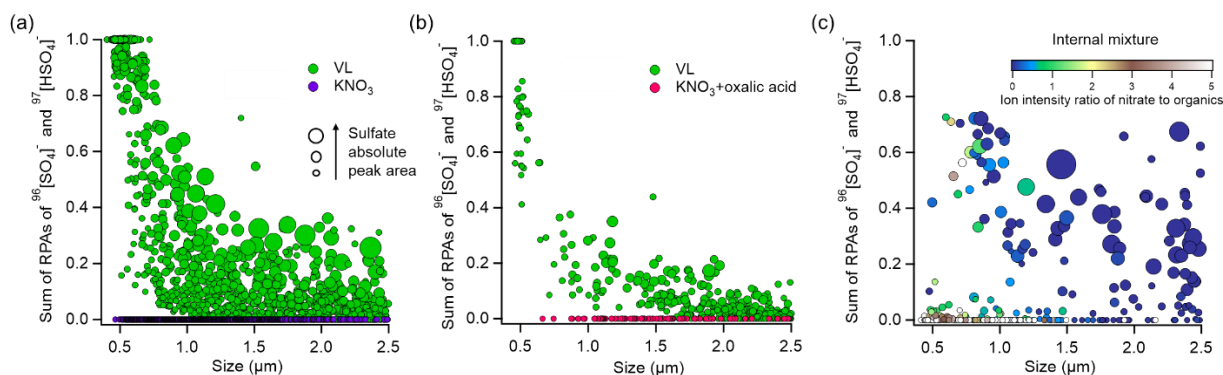


Figure 4. Sulfate RPA vs. particle diameter detected by the SPAMS for (a) externally mixed VL-coated particles and KNO_3 ; (b) externally mixed VL-coated particles and KNO_3 -oxalic acid particles; and (c) internally mixed VL and KNO_3 particles at 80% RH under UV irradiation (I_1) in the presence of SO_2 . The markers are presented as a function of sulfate APA. The color scale in c indicates the ion intensity ratio of nitrate to organics (total negative ion intensity subtracted by nitrate and sulfate intensity) in the negative mass spectra.

Data availability. The data are available upon request to the corresponding author.

Author contributions. CKC and LZ designed the experiment; LZ and ZL conducted the experiments; LZ and ZL performed the data interpretation; LZ, ZL, BRGM, RAIC, RT, ML, CC and CKC wrote the paper. All authors contributed to the paper with useful scientific discussions or comments.

Competing interests. The contact author has declared that neither they nor their co-authors have any competing interests.

Acknowledgements. We gratefully acknowledge the support from the Hong Kong Research Grants Council (No.11304121, R1016-20F) and the National Natural Science Foundation of China (No. 42275104).

338 **References**

- 339 Alexander, B., Park, R. J., Jacob, D. J., and Gong, S.: Transition metal-catalyzed oxidation of atmospheric sulfur: Global
340 implications for the sulfur budget, *Journal of Geophysical Research: Atmospheres*, 114, 2009.
- 341 Anastasio, C., Faust, B. C., and Rao, C. J.: Aromatic carbonyl compounds as aqueous-phase photochemical sources of
342 hydrogen peroxide in acidic sulfate aerosols, fogs, and clouds. 1. Non-phenolic methoxybenzaldehydes and
343 methoxyacetophenones with reductants (phenols), *Environmental science & technology*, 31, 218-232, 1996.
- 344 Calvert, J. G., BOTTENHEIM, J. W., and STRAUSZ, O. P.: Mechanism of the homogeneous oxidation of sulfur dioxide in
345 the troposphere, in: *Sulfur in the Atmosphere*, Elsevier, 197-226, 1978.
- 346 Canonica, S., Jans, U., Stemmler, K., and Hoigne, J.: Transformation kinetics of phenols in water: photosensitization by
347 dissolved natural organic material and aromatic ketones, *Environmental science & technology*, 29, 1822-1831, 1995.
- 348 Chan, C. K., and Yao, X.: Air pollution in mega cities in China, *Atmospheric environment*, 42, 1-42, 2008.
- 349 Chen, C.-H., Tsai, C.-Y., Chen, T.-F., Hou, L.-S., and Chang, K.-H.: Temporal Trends and Spatial Distribution Characteristics
350 of Air Quality Monitored in China from 2015 to 2020, *Journal of Innovative Technology*, 4, 23-28, 2022.
- 351 Chen, Y., Li, N., Li, X., Tao, Y., Luo, S., Zhao, Z., Ma, S., Huang, H., Chen, Y., and Ye, Z.: Secondary organic aerosol
352 formation from 3C*-initiated oxidation of 4-ethylguaiacol in atmospheric aqueous-phase, *Science of The Total Environment*,
353 723, 137953, 2020.
- 354 Cheng, C., Li, M., Chan, C. K., Tong, H., Chen, C., Chen, D., Wu, D., Li, L., Wu, C., and Cheng, P.: Mixing state of oxalic
355 acid containing particles in the rural area of Pearl River Delta, China: implications for the formation mechanism of oxalic acid,
356 *Atmospheric Chemistry and Physics*, 17, 9519-9533, 2017.
- 357 Cheng, Y., Zheng, G., Wei, C., Mu, Q., Zheng, B., Wang, Z., Gao, M., Zhang, Q., He, K., and Carmichael, G.: Reactive
358 nitrogen chemistry in aerosol water as a source of sulfate during haze events in China, *Science advances*, 2, e1601530, 2016.
- 359 Corral Arroyo, P., Bartels-Rausch, T., Alpert, P. A., Dumas, S. p., Perrier, S. b., George, C., and Ammann, M.: Particle-phase
360 photosensitized radical production and aerosol aging, *Environmental science & technology*, 52, 7680-7688, 2018.
- 361 Dalrymple, R. M., Carfagno, A. K., and Sharpless, C. M.: Correlations between dissolved organic matter optical properties
362 and quantum yields of singlet oxygen and hydrogen peroxide, *Environmental science & technology*, 44, 5824-5829, 2010.
- 363 Felber, T., Schaefer, T., He, L., and Herrmann, H.: Aromatic Carbonyl and Nitro Compounds as Photosensitizers and Their
364 Photophysical Properties in the Tropospheric Aqueous Phase, *The Journal of Physical Chemistry A*, 125, 5078-5095, 2021.
- 365 Freney, E. J., Martin, S. T., and Buseck, P. R.: Deliquescence and efflorescence of potassium salts relevant to biomass-burning
366 aerosol particles, *Aerosol Science and Technology*, 43, 799-807, 2009.
- 367 Fuzzi, S., Baltensperger, U., Carslaw, K., Decesari, S., Denier van der Gon, H., Facchini, M. C., Fowler, D., Koren, I.,
368 Langford, B., and Lohmann, U.: Particulate matter, air quality and climate: lessons learned and future needs, *Atmospheric
369 chemistry and physics*, 15, 8217-8299, 2015.
- 370 Gen, M., Zhang, R., Huang, D. D., Li, Y., and Chan, C. K.: Heterogeneous SO₂ oxidation in sulfate formation by photolysis
371 of particulate nitrate, *Environmental Science & Technology Letters*, 6, 86-91, 2019a.

372 Gen, M., Zhang, R., Huang, D. D., Li, Y., and Chan, C. K.: Heterogeneous oxidation of SO₂ in sulfate production during
373 nitrate photolysis at 300 nm: effect of pH, relative humidity, irradiation intensity, and the presence of organic compounds,
374 *Environmental Science & Technology*, 53, 8757-8766, 2019b.

375 Gen, M., Liang, Z., Zhang, R., Mabato, B. R. G., and Chan, C. K.: Particulate nitrate photolysis in the atmosphere,
376 *Environmental Science: Atmospheres*, 2022.

377 George, C., Ammann, M., D'Anna, B., Donaldson, D., and Nizkorodov, S. A.: Heterogeneous photochemistry in the
378 atmosphere, *Chemical reviews*, 115, 4218-4258, 2015.

379 George, C., Brüggemann, M., Hayeck, N., Tinel, L., and Donaldson, J.: Interfacial Photochemistry, in: *Physical Chemistry of*
380 *Gas-Liquid Interfaces*, Elsevier, 435-457, 2018.

381 González Palacios, L., Corral Arroyo, P., Aregahegn, K. Z., Steimer, S. S., Bartels-Rausch, T., Nozière, B., George, C.,
382 Ammann, M., and Volkamer, R.: Heterogeneous photochemistry of imidazole-2-carboxaldehyde: HO₂ radical formation and
383 aerosol growth, *Atmospheric Chemistry and Physics*, 16, 11823-11836, 2016.

384 Grantz, D., Garner, J., and Johnson, D.: Ecological effects of particulate matter, *Environment international*, 29, 213-239, 2003.

385 Gross, D. S., Gälli, M. E., Silva, P. J., and Prather, K. A.: Relative sensitivity factors for alkali metal and ammonium cations
386 in single-particle aerosol time-of-flight mass spectra, *Analytical Chemistry*, 72, 416-422, 2000.

387 Guazzotti, S. A., Coffee, K. R., and Prather, K. A.: Continuous measurements of size-resolved particle chemistry during
388 INDOEX-Intensive Field Phase 99, *Journal of Geophysical Research: Atmospheres*, 106, 28607-28627, 2001.

389 Harris, E., Sinha, B., Van Pinxteren, D., Tilgner, A., Fomba, K. W., Schneider, J., Roth, A., Gnauk, T., Fahlbusch, B., and
390 Mertes, S.: Enhanced role of transition metal ion catalysis during in-cloud oxidation of SO₂, *Science*, 340, 727-730, 2013.

391 Hatch, L. E., Pratt, K. A., Huffman, J. A., Jimenez, J. L., and Prather, K. A.: Impacts of aerosol aging on laser
392 desorption/ionization in single-particle mass spectrometers, *Aerosol Science and Technology*, 48, 1050-1058, 2014.

393 Hoffmann, M. R., and Calvert, J. G.: Chemical Transformation Modules for Eulerian Acid Deposition Models: Volume II, the
394 *Aqueous-phase Chemistry*, EPA/600/3-85, 17, 1985.

395 Hu, X., Guo, Z., Sun, W., Lian, X., Fu, Y., Meng, H., Zhu, Y., Zhang, G., Wang, X., and Xue, L.: Atmospheric Processing of
396 Particulate Imidazole Compounds Driven by Photochemistry, *Environmental Science & Technology Letters*, 9, 265-271, 2022.

397 Hudda, N., and Fruin, S.: International airport impacts to air quality: size and related properties of large increases in ultrafine
398 particle number concentrations, *Environmental science & technology*, 50, 3362-3370, 2016.

399 Hussain, K., Thorsen, G., and Malthe-Sørensen, D.: Nucleation and metastability in crystallization of vanillin and ethyl
400 vanillin, *Chemical engineering science*, 56, 2295-2304, 2001.

401 Ibusuki, T., and Takeuchi, K.: Sulfur dioxide oxidation by oxygen catalyzed by mixtures of manganese (II) and iron (III) in
402 aqueous solutions at environmental reaction conditions, *Atmospheric Environment* (1967), 21, 1555-1560, 1987.

403 Jahn, L. G., Jahl, L. G., Bowers, B. B., and Sullivan, R. C.: Morphology of organic carbon coatings on biomass-burning
404 particles and their role in reactive gas uptake, *ACS Earth and Space Chemistry*, 5, 2184-2195, 2021.

405 Kaur, R., and Anastasio, C.: First measurements of organic triplet excited states in atmospheric waters, *Environmental science*
406 *& technology*, 52, 5218-5226, 2018.

407 Kaur, R., Labins, J. R., Helbock, S. S., Jiang, W., Bein, K. J., Zhang, Q., and Anastasio, C.: Photooxidants from brown carbon
408 and other chromophores in illuminated particle extracts, *Atmospheric Chemistry and Physics*, 19, 6579-6594, 2019.

409 Kavuru, P., Grebinoski, S. J., Patel, M. A., Wojtas, L., and Chadwick, K.: Polymorphism of vanillin revisited: the discovery
410 and selective crystallization of a rare crystal structure, *CrystEngComm*, 18, 1118-1122, 2016.

411 Kroll, J. A., Frandsen, B. N., Kjaergaard, H. G., and Vaida, V.: Atmospheric hydroxyl radical source: Reaction of triplet SO₂
412 and water, *The Journal of Physical Chemistry A*, 122, 4465-4469, 2018.

413 Li, L., Huang, Z., Dong, J., Li, M., Gao, W., Nian, H., Fu, Z., Zhang, G., Bi, X., and Cheng, P.: Real time bipolar time-of-
414 flight mass spectrometer for analyzing single aerosol particles, *International Journal of Mass Spectrometry*, 303, 118-124,
415 2011.

416 Li, Y. J., Yeung, J. W., Leung, T. P., Lau, A. P., and Chan, C. K.: Characterization of organic particles from incense burning
417 using an aerodyne high-resolution time-of-flight aerosol mass spectrometer, *Aerosol science and technology*, 46, 654-665,
418 2012.

419 Liang, Z., Zhou, L., Infante Cuevas, R. A., Li, X., Cheng, C., Li, M., Tang, R., Zhang, R., Lee, P. K., and Lai, A. C.: Sulfate
420 Formation in Incense Burning Particles: A Single-Particle Mass Spectrometric Study, *Environmental Science & Technology*
421 Letters, 2022.

422 Liu, T., and Abbatt, J. P.: An experimental assessment of the importance of S (IV) oxidation by hypohalous acids in the marine
423 atmosphere, *Geophysical Research Letters*, 47, e2019GL086465, 2020.

424 Liu, T., Clegg, S. L., and Abbatt, J. P.: Fast oxidation of sulfur dioxide by hydrogen peroxide in deliquesced aerosol particles,
425 *Proceedings of the National Academy of Sciences*, 117, 1354-1359, 2020.

426 Liu, T., and Abbatt, J. P.: Oxidation of sulfur dioxide by nitrogen dioxide accelerated at the interface of deliquesced aerosol
427 particles, *Nature Chemistry*, 13, 1173-1177, 2021.

428 Liu, T., Chan, A. W., and Abbatt, J. P.: Multiphase oxidation of sulfur dioxide in aerosol particles: implications for sulfate
429 formation in polluted environments, *Environmental Science & Technology*, 55, 4227-4242, 2021.

430 Liu, W., and Sun, S.: Ultrastructural changes of tracheal epithelium and alveolar macrophages of rats exposed to mosquito coil
431 smoke, *Toxicology letters*, 41, 145-157, 1988.

432 Mabato, B. R. G., Lyu, Y., Ji, Y., Li, Y. J., Huang, D. D., Li, X., Nah, T., Lam, C. H., and Chan, C. K.: Aqueous secondary
433 organic aerosol formation from the direct photosensitized oxidation of vanillin in the absence and presence of ammonium
434 nitrate, *Atmospheric Chemistry and Physics*, 22, 273-293, 2022.

435 Mabato, B. R. G., Li, Y. J., Huang, D. D., Wang, Y., and Chan, C. K.: Comparison of aqueous secondary organic aerosol
436 (aqSOA) product distributions from guaiacol oxidation by non-phenolic and phenolic methoxybenzaldehydes as
437 photosensitizers in the absence and presence of ammonium nitrate, *Atmospheric Chemistry and Physics* 23, 2859-2875, 2023.

438 Martin, L. R., and Good, T. W.: Catalyzed oxidation of sulfur dioxide in solution: The iron-manganese synergism, *Atmospheric*
439 *Environment. Part A. General Topics*, 25, 2395-2399, 1991.

440 Martins-Costa, M. T., Anglada, J. M., Francisco, J. S., and Ruiz-López, M. F.: Photochemistry of SO₂ at the air–water
441 interface: a source of OH and HOSO radicals, *Journal of the American Chemical Society*, 140, 12341-12344, 2018.

442 Mochida, M., and Kawamura, K.: Hygroscopic properties of levoglucosan and related organic compounds characteristic to
443 biomass burning aerosol particles, *Journal of Geophysical Research: Atmospheres*, 109, 2004.

444 Mochizuki, T., Kawamura, K., Miyazaki, Y., Wada, R., Takahashi, Y., Saigusa, N., and Tani, A.: Secondary formation of
 445 oxalic acid and related organic species from biogenic sources in a larch forest at the northern slope of Mt. Fuji, Atmospheric
 446 environment, 166, 255-262, 2017.

447 Nel, A.: Air pollution-related illness: effects of particles, Science, 308, 804-806, 2005.

448 Neubauer, K. R., Johnston, M. V., and Wexler, A. S.: Humidity effects on the mass spectra of single aerosol particles,
 449 Atmospheric Environment, 32, 2521-2529, 1998.

450 Nolte, C. G., Schauer, J. J., Cass, G. R., and Simoneit, B. R.: Highly polar organic compounds present in wood smoke and in
 451 the ambient atmosphere, Environmental science & technology, 35, 1912-1919, 2001.

452 Peng, D.-Q., Yu, Z.-X., Wang, C.-H., Gong, B., Liu, Y.-Y., and Wei, J.-H.: Chemical Constituents and Anti-Inflammatory
 453 Effect of Incense Smoke from Agarwood Determined by GC-MS, International Journal of Analytical Chemistry, 2020, 2020.

454 Pratt, K. A., Mayer, J. E., Holecek, J. C., Moffet, R. C., Sanchez, R. O., Rebotier, T. P., Furutani, H., Gonin, M., Fuhrer, K.,
 455 and Su, Y.: Development and characterization of an aircraft aerosol time-of-flight mass spectrometer, Analytical chemistry,
 456 81, 1792-1800, 2009.

457 Qi, C., Stanley, N., Pui, D. Y., and Kuehn, T. H.: Laboratory and on-road evaluations of cabin air filters using number and
 458 surface area concentration monitors, Environmental science & technology, 42, 4128-4132, 2008.

459 Qi, X., Pang, X., Hong, Y., Wang, Y., Lou, S., Feng, J., Cheng, P., and Zhou, Z.: Real-time analysis of the homogeneous and
 460 heterogeneous reactions of pyrene with ozone by SPAMS and CRD-EAS, Chemosphere, 234, 608-617, 2019.

461 Reinard, M. S., and Johnston, M. V.: Ion formation mechanism in laser desorption ionization of individual nanoparticles,
 462 Journal of the American Society for Mass Spectrometry, 19, 389-399, 2008.

463 Rogge, W. F., Hildemann, L. M., Mazurek, M. A., Cass, G. R., and Simoneit, B. R.: Sources of fine organic aerosol. 9. Pine,
 464 oak, and synthetic log combustion in residential fireplaces, Environmental Science & Technology, 32, 13-22, 1998.

465 Rubasinghege, G., and Grassian, V. H.: Role (s) of adsorbed water in the surface chemistry of environmental interfaces,
 466 Chemical Communications, 49, 3071-3094, 2013.

467 Schauer, J. J., Kleeman, M. J., Cass, G. R., and Simoneit, B. R.: Measurement of emissions from air pollution sources. 3. C1–
 468 C29 organic compounds from fireplace combustion of wood, Environmental science & technology, 35, 1716-1728, 2001.

469 Simoneit, B. R., Rogge, W., Mazurek, M., Standley, L., Hildemann, L., and Cass, G.: Lignin pyrolysis products, lignans, and
 470 resin acids as specific tracers of plant classes in emissions from biomass combustion, Environmental science & technology,
 471 27, 2533-2541, 1993.

472 Smith, J. D., Sio, V., Yu, L., Zhang, Q., and Anastasio, C.: Secondary organic aerosol production from aqueous reactions of
 473 atmospheric phenols with an organic triplet excited state, Environmental science & technology, 48, 1049-1057, 2014.

474 Smith, J. D., Kinney, H., and Anastasio, C.: Aqueous benzene-diols react with an organic triplet excited state and hydroxyl
 475 radical to form secondary organic aerosol, Physical Chemistry Chemical Physics, 17, 10227-10237, 2015.

476 Smith, J. D., Kinney, H., and Anastasio, C.: Phenolic carbonyls undergo rapid aqueous photodegradation to form low-volatility,
 477 light-absorbing products, Atmospheric Environment, 126, 36-44, 2016.

478 Walcek, C. J., and Taylor, G. R.: A theoretical method for computing vertical distributions of acidity and sulfate production
 479 within cumulus clouds, Journal of Atmospheric Sciences, 43, 339-355, 1986.

480 Wang, G., Zhang, R., Gomez, M. E., Yang, L., Levy Zamora, M., Hu, M., Lin, Y., Peng, J., Guo, S., and Meng, J.: Persistent
481 sulfate formation from London Fog to Chinese haze, *Proceedings of the National Academy of Sciences*, 113, 13630-13635,
482 2016.

483 Wang, X., Gemayel, R., Hayeck, N., Perrier, S., Charbonnel, N., Xu, C., Chen, H., Zhu, C., Zhang, L., and Wang, L.:
484 Atmospheric photosensitization: a new pathway for sulfate formation, *Environmental Science & Technology*, 54, 3114-3120,
485 2020.

486 Wang, X., Gemayel, R., Baboornian, V. J., Li, K., Boreave, A., Dubois, C., Tomaz, S., Perrier, S., Nizkorodov, S. A., and
487 George, C.: Naphthalene-Derived Secondary Organic Aerosols Interfacial Photosensitizing Properties, *Geophysical Research*
488 *Letters*, 48, e2021GL093465, 2021.

489 Wang, Y., Zhang, Q., Jiang, J., Zhou, W., Wang, B., He, K., Duan, F., Zhang, Q., Philip, S., and Xie, Y.: Enhanced sulfate
490 formation during China's severe winter haze episode in January 2013 missing from current models, *Journal of Geophysical*
491 *Research: Atmospheres*, 119, 10,425-410,440, 2014.

492 Willeke, K., and Whitby, K. T.: Atmospheric aerosols: size distribution interpretation, *Journal of the Air Pollution Control*
493 *Association*, 25, 529-534, 1975.

494 Yang, F., Chen, H., Wang, X., Yang, X., Du, J., and Chen, J.: Single particle mass spectrometry of oxalic acid in ambient
495 aerosols in Shanghai: Mixing state and formation mechanism, *Atmospheric Environment*, 43, 3876-3882, 2009.

496 Yao, M., Zhao, Y., Hu, M., Huang, D., Wang, Y., Yu, J. Z., and Yan, N.: Multiphase reactions between secondary organic
497 aerosol and sulfur dioxide: kinetics and contributions to sulfate formation and aerosol aging, *Environmental Science &*
498 *Technology Letters*, 6, 768-774, 2019.

499 Ye, J., Abbatt, J. P., and Chan, A. W.: Novel pathway of SO₂ oxidation in the atmosphere: reactions with monoterpene
500 ozonolysis intermediates and secondary organic aerosol, *Atmospheric Chemistry and Physics*, 18, 5549-5565, 2018.

501 Zauscher, M. D., Wang, Y., Moore, M. J., Gaston, C. J., and Prather, K. A.: Air quality impact and physicochemical aging of
502 biomass burning aerosols during the 2007 San Diego wildfires, *Environmental science & technology*, 47, 7633-7643, 2013.

503 Zhang, R., Wang, G., Guo, S., Zamora, M. L., Ying, Q., Lin, Y., Wang, W., Hu, M., and Wang, Y.: Formation of urban fine
504 particulate matter, *Chemical reviews*, 115, 3803-3855, 2015.

505 Zhang, R., Gen, M., Huang, D., Li, Y., and Chan, C. K.: Enhanced sulfate production by nitrate photolysis in the presence of
506 halide ions in atmospheric particles, *Environmental Science & Technology*, 54, 3831-3839, 2020.

507 Zhang, Y., Zhang, X., Sun, J., Hu, G., Shen, X., Wang, Y., Wang, T., Wang, D., and Zhao, Y.: Chemical composition and
508 mass size distribution of PM₁ at an elevated site in central east China, *Atmospheric Chemistry and Physics*, 14, 12237-12249,
509 2014.

510 Zhang, Y., Li, W., Li, L., Li, M., Zhou, Z., Yu, J., and Zhou, Y.: Source apportionment of PM_{2.5} using PMF combined online
511 bulk and single-particle measurements: Contribution of fireworks and biomass burning, *Journal of Environmental Sciences*,
512 2022.

513 Zheng, B., Zhang, Q., Zhang, Y., He, K., Wang, K., Zheng, G., Duan, F., Ma, Y., and Kimoto, T.: Heterogeneous chemistry:
514 a mechanism missing in current models to explain secondary inorganic aerosol formation during the January 2013 haze episode
515 in North China, *Atmospheric Chemistry and Physics*, 15, 2031-2049, 2015.

516 Zhou, L., Li, M., Cheng, C., Zhou, Z., Nian, H., Tang, R., and Chan, C. K.: Real-time chemical characterization of single
517 ambient particles at a port city in Chinese domestic emission control area—Impacts of ship emissions on urban air quality,
518 Science of the Total Environment, 819, 153117, 2022.

519 Zhou, Y., Huang, X. H., Griffith, S. M., Li, M., Li, L., Zhou, Z., Wu, C., Meng, J., Chan, C. K., and Louie, P. K.: A field
520 measurement based scaling approach for quantification of major ions, organic carbon, and elemental carbon using a single
521 particle aerosol mass spectrometer, Atmospheric Environment, 143, 300-312, 2016.

522 Zuend, A., Marcolli, C., Luo, B. P., and Peter, T.: A thermodynamic model of mixed organic-inorganic aerosols to predict
523 activity coefficients, Atmospheric Chemistry and Physics, 8, 4559-4593, 2008.

524